IIETA International Information and Engineering Technology Association
Advancing the World of Information and Engineering

Mathematical Modelling of Engineering Problems
Vol. 13, No. 2, February, 2026, pp. 321-333
Journal homepage: http://iieta.org/journals/mmep

Numerical Punching Shear Analysis of Truss-Shear Reinforced Flat Slabs on Rectangular Columns

Hussein Riyadh Taresh[1*], Thamer Hussein Amer[1], Mohd Yazmil Md Yatim[2]

[1] College of Engineering, University of Sumer, Rifai 64005, Iraq
[2] Department of Civil Engineering, Universiti Kebangsaan Malaysia, UKM Bangi 43600, Malaysia

Corresponding Author Email: Hussein.Riyadh@uos.edu.iq

https://doi.org/10.18280/mmep.130209

Received: 25 November 2025
Revised: 20 January 2026
Accepted: 30 January 2026
Available online: 15 March 2026

Keywords:
flat slabs, punching shear, rectangular columns, truss-type shear reinforcement, nonlinear finite element analysis, punching shear design

ABSTRACT

This study investigates the punching shear behaviour of flat slabs using a finite element approach. Various truss-shear reinforcement configurations were examined to enhance punching shear resistance and avoid brittle failure. The flat slab models demonstrated non-uniform shear transmission due to the inclusion of rectangular column capitals. The numerical analysis indicated a significant increase of approximately 79% in punching strength for the shear-reinforced slabs compared to the reference slab. The shear reinforcements changed the failure mode from punching shear to flexural failure with minimal changes, resulting in enhanced ductility, stiffness, and energy absorption. The square truss-shear reinforcement performed better than triangular alternatives, providing greater stability and stronger support for the flexural bars. The diagonal reinforcing bars markedly improved punching shear resistance, as evidenced by significantly higher stresses at ultimate load. The numerically obtained results were compared with punching shear strengths specified in design codes ACI 318-19 and Eurocode 2.

1. INTRODUCTION

A flat slab construction system is commonly used to create large open spaces, such as parking garages, where cast-in-place reinforced concrete slabs are supported by either cast-in-place or precast reinforced concrete columns with capitals, sometimes supplemented with drop panels. The columns are affixed to the bottom floor slab using steel bolts and subsequently enclosed in concrete for protection. Column capitals are positioned above the columns to expand the connection zone for enhancing resistance against brittle punching shear failure. This type of failure occurs when the shear stresses exceed the concrete's tensile resistance around the column or column capital. Different span lengths in the two orthogonal orientations of the flat slab cause column capitals to be rectangular. This design reduces negative moments around column capitals by shortening the span. Moreover, rectangular column capitals often feature rounded corners to minimise shear stress concentration at the corners.

Previous studies have identified two primary limitations in the punching shear strength of flat slabs supported by rectangular columns [1-4]. Firstly, the distribution of concrete shear stresses over rectangular columns is not always uniform. As a result, the corners of the column, rather than its sides, experience higher shear stresses. Since the shear stresses along the longer sides of a rectangular column are lower than those at the corners, this unequal shear transmission becomes more pronounced in flat slabs supported by such columns. Secondly, shear and flexural cracks in the flat slab often manifest earlier along the shorter side of the column owing to elevated shear pressures and bending moments relative to the longer side. This indicates that the arrangement and configuration of shear reinforcement may influence punching shear resistance, particularly if shear transfer is inconsistent in both orthogonal directions.

The provisions in ACI 318-19 [5] related to punching shear design are based on experimental investigations by studies [6-8] specifically focusing on slabs without shear enhancement. Studies [9, 10] suggested empirical equations for the European Eurocode 2 [11]. Eurocode 2 takes into consideration both the strength of concrete and the strength of flexural reinforcement. ACI 318-19 only looks at the strength of concrete. Also, Eurocode 2 defines the critical section, where shear and bending stresses reach their maximum levels, at two times the effective depth of the slab ($2d$) from the column face, whereas ACI 318-19 specifies it at $0.5d$ from the column face. Researchers have systematically investigated various shear reinforcement types, such as bent-up bars [12, 13] and closed stirrups [14-17], shear heads [18-20], and shear studs [21, 22].

A crucial aspect of structural design involves making sure that flat slabs do not fail because of punching shear. Traditional techniques, like stirrups and shear heads, are not always simple to implement. For instance, stirrups should engage the flexural reinforcing bars through hooks to function properly. This complicates installation and makes radial arrangement more challenging. Alternatively, truss-shear reinforcement (truss bars or bar trusses) represents a more efficient alternative [23-25]. A truss-shear reinforcement is

made up of horizontal top and bottom chord bars interconnected by transverse vertical and diagonal bars (Figure 1). The vertical and diagonal bar trusses play a crucial role in preventing punching failure by intersecting diagonal shear cracks [26].

A major gap still exists. Although it is well-known that truss-shear reinforcement is generally effective, the effects of its geometry and placement on punching shear resistance and failure modes are still not understood. The limited understanding of the detailed mechanics of this truss-shear reinforcement concept leaves practitioners uncertain about the implementation of reinforcement strategies, which in turn hampers a broader acceptance and application of that practical system to engineering practice.

This research systematically investigates the relationship between truss-shear reinforcement parameters and the structural performance of flat slabs. This work primarily innovates by quantifying the impact of variations in truss geometry and configuration on ultimate punching strength and the associated failure mode. This study's findings aim to furnish essential data for the development of performance-based design guidelines, thereby enhancing the confident and efficient application of truss-type shear reinforcement in practical scenarios.

Four slab specimens, deep slab with no shear reinforcement (DSN), deep slab with single-leg stirrups (DSS), deep slabs with trusses (DST1 and DST2), representing slab-column interior connections, were selected for this numerical study. They were tested by Eom et al. [26] under static loading. Slab specimen DSN had no shear reinforcement, whilst slab specimen DSS was reinforced with typical single-leg D10 stirrups with 90° and 135° end hooks. In contrast, slabs DST1 and DST2 were reinforced using triangular trusses. All the tested slabs underwent model calibration using the finite element simulation, serving as benchmark models for further parametric investigations to achieve the aims of the study. The numerical results were then compared with code-based predictions of punching shear strength.

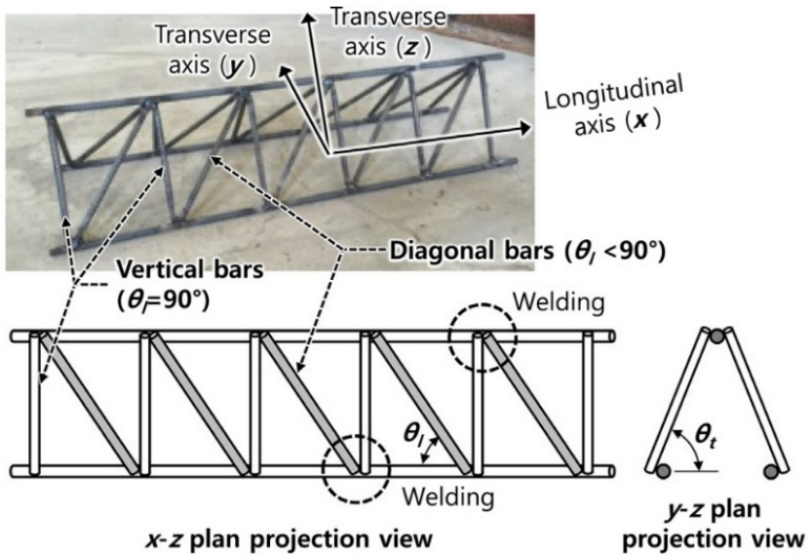

Figure 1. Details of preassembled bar truss [26]

2. DESCRIPTION OF TEST SLABS

Slabs DSN, DSS, DST1, and DST2 tested by Eom et al. [26] were selected as finite element benchmark models following proper calibration using the ABAQUS software package [27]. These slabs represent interior slab-column connections in a typical flat slab system. The slabs were subjected to punching shear loading through the lower column stubs and supported along their edges, where bending moments vanish (contraflexure boundaries). The column corners were semi-circular with a diameter of 180 mm, whilst the four corners of the column capital were quarter-circles with a radius of 90 mm. The top tension reinforcement ratio was ρ_{ly} = 0.0163 along the *y*-direction, whilst ρ_{lx} = 0.009 along the *x*-direction. These reinforcement ratios were chosen to provide an ultimate flexural strength of 2382 kN. The average effective depth of the slab was taken as d = 206 mm. Figure 2 presents a typical geometry and details of reinforcement for the test slabs.

The control slab DSN, as shown in Figure 3(a), was not provided with any shear reinforcement. Slab DSS was reinforced using single-leg stirrups, which engaged both the top and bottom flexural bars as illustrated in Figure 3(b). Slabs DST1 and DST2 were reinforced against punching shear using triangular trusses. Specifically, slab DST1 was reinforced with two trusses placed orthogonally in each direction around the column capital as shown in Figure 3(c). In contrast, slab DST2 was reinforced with eight triangular trusses arranged radially around the column capital as presented in Figure 3(d). These trusses were positioned between the tension and compression flexural reinforcement mats. Other key details of the stirrups and trusses are illustrated in Figure 3.

The material properties of the test slabs are summarised in Table 1. Since the tensile strength and modulus of elasticity of concrete were not reported in the original study, they were estimated using the ACI 318-19 approach. The maximum aggregate size used in the concrete mix was 25 mm. All slabs were tested using a hydraulic jack with a maximum stroke of 300 mm. The slabs were supported along their edges in a manner that prevented the corners from uplifting throughout the test. Slab deflections were determined by averaging the readings from LVDT1 and LVDT2, which were positioned at the column's rounded edges. Further detailed information can be found in reference [26].

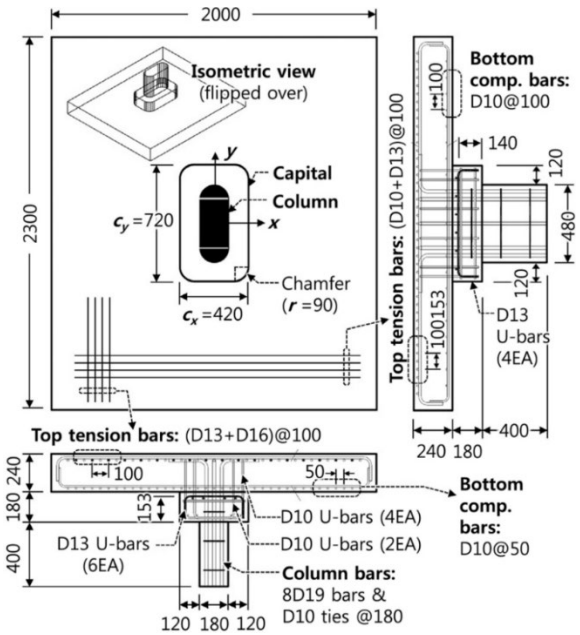

Figure 2. Typical geometry and reinforcement details of test slabs [26]

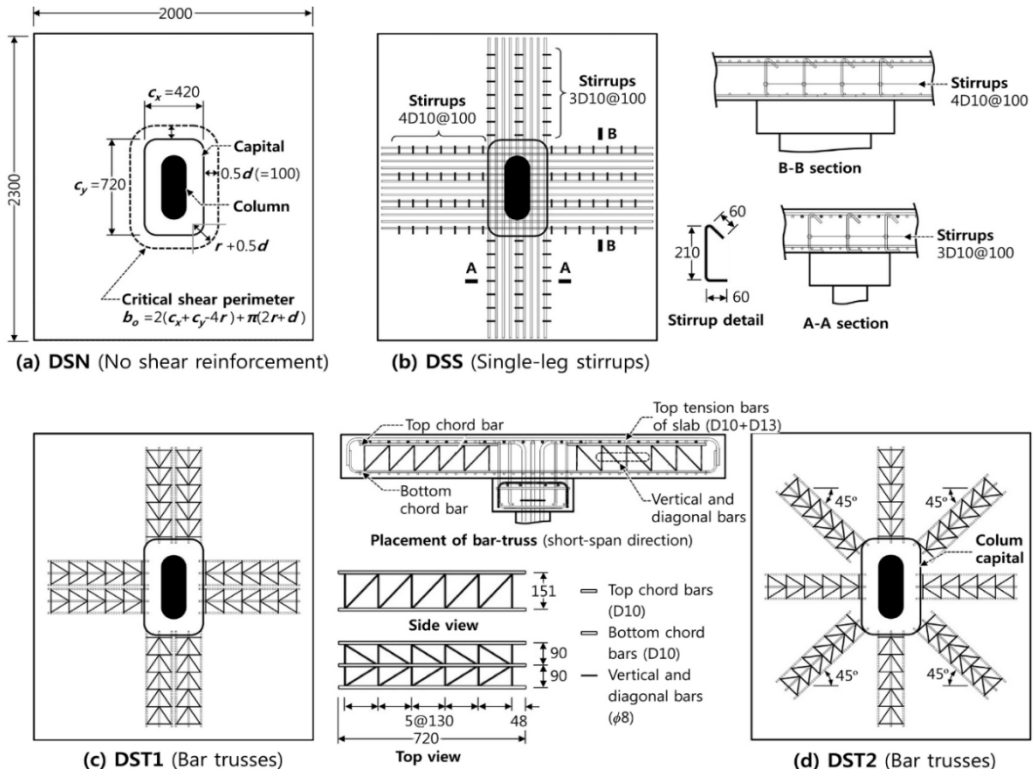

Figure 3. Shear reinforcement details [26]

Table 1. Material properties of the test slabs [26]

Slab Elements	Concrete Compressive Strength f'_c (MPa)	Concrete Tensile Strength f'_t (MPa)	Reinforcement Yield Strength f_{yt} (MPa)	Modulus of Elasticity E_c (GPa)
Concrete (slabs DSN & DSS)	31.8	1.86*	–	26.50*
Concrete (slabs DST1 & DST2)	32.4	1.88*	–	26.75*
D10 reinforcing bars	–	–	595	200
D13 reinforcing bars	–	–	552	200
D16 reinforcing bars	–	–	614	200
D19 reinforcing bars	–	–	617	200
D10 chord bars	–	–	535	200
D8 vertical/diagonal bar trusses	–	–	609	200

Note: *Estimated based on the ACI 318-19 approach.

3. FINITE ELEMENT CALIBRATION OF TEST SLABS

3.1 Calibration process

A three-dimensional non-linear analysis was conducted using the ABAQUS finite element package to evaluate the response of test slabs (DSN, DSS, DST1, and DST2) under static shear-punching loads. The Concrete Damaged Plasticity (CDP) model [28-31] was employed to simulate the non-linear behaviour of the concrete slabs for capturing inelastic deformation, cracking, crushing, and stiffness degradation. The concrete was modelled using 8-node hexahedral brick elements (C3D8R) with reduced integration [32-35].

The compressive response of concrete was modelled using the Hognestad parabola, whilst the tensile response was defined by a stress-crack displacement relationship rather than a stress-strain relationship. This tensile behaviour was characterised by a bilinear tension-softening response, which requires essential concrete parameters such as the fracture energy G_f and the maximum tensile strength f'_t. Parameter G_f represents the area under the tensile stress-crack displacement curve and is influenced by aggregate size and concrete quality. It can be estimated following the Euro-International Committee for Concrete - International Federation for Prestressing (CEB-FIP Model Code 1990) [36]. Accordingly, the fracture energy was determined using Eq. (1).

$$G_f = G_{fo}(f_{cm}/f_{cmo})^{0.7} \quad (1)$$

where, f_{cm} = mean compressive strength of concrete, f_{cmo} = 10 MPa, and G_{fo} is the base fracture energy that depends on the maximum aggregate size (d_g), taken as 0.045 N/mm in the present study.

All reinforcing bars (flexural bars, single-leg stirrups, and trusses) were modelled by using truss elements (T3D2). The key advantage of using such an element type is its ability to resist tensile or compressive loads, as they exhibit minimal resistance to bending due to possessing only three translational degrees of freedom [27]. However, a recent study used this element type for modelling such reinforcements [37]. The elastic behaviour of all these reinforcements was defined with a Poisson's ratio v of 0.3 and a Young's modulus Es of 200 GPa. The plastic behaviour was defined using a data Table 2 that presented yield stress alongside the associated plastic strain. The embedding approach was used to simulate the bond between all these reinforcements and the concrete. The plastic behaviour was specified through a data table that included yield stress and the corresponding plastic strain.

Table 2. Used damaged plasticity parameters

Damaged Plasticity Parameters	Value
Concrete Poisson's ratio v	0.2
Steel Poisson's ratio v	0.3
Dilation angle ψ (°)	40
Ratio of stress invariants K_c	0.667
Ratio of initial equibiaxial to initial uniaxial compressive yield stresses σ_{bo}/σ_{co}	1.16
Viscosity parameter μ	0
Eccentricity ε	0.1

In the CDP model, the default values of K_c, σ_{bo}/σ_{co}, and ε are 0.667, 1.16, and 0.1, respectively, based on the study [27] and extensive previous numerical investigations using the CDP model in ABAQUS [30-35]. As the quasi-static analysis is used, the viscous regularisation parameter μ in the CDP model was assumed to be 0 [30-35]. The dilation angle ψ was set to 45° [31], representing inelastic volumetric changes within the model. Since the loading was monotonic, compression and tension damage parameters were disregarded. Sensitive analyses were conducted regarding the mesh size and dilation angle, as shown in Figure 4.

Quasi-static analysis in ABAQUS was employed to analyse the experimental slabs. This method requires the application of a low velocity to ensure accurate results. All slab models were assigned a displacement rate of 20 mm/s, which was incrementally increased following a smooth amplitude curve from 0 mm/s to 40 mm/s. Restraints were strategically positioned at the upper edges of the slabs, corresponding to the direction of the applied force. Figure 5 shows the typical geometry and boundary conditions of the slab models used in the simulations. The slab deflection Δ was determined as the average value of the deflections at the rounded edges of the column. A finite element sensitivity study was conducted using mesh sizes of 30 mm, 36 mm, and 40 mm, ensuring that each exceeded the aggregate size of 25 mm whilst remaining sufficiently small to prevent a coarse mesh. Based on this study, a 36 mm mesh size was selected for the calibration process. This decision was based on the convergence of results and the agreement between finite element and experimental observations, particularly in terms of load-deflection responses, cracking patterns, and flexural reinforcement behaviour. Figure 6 shows the load-deflection curves for all slab models.

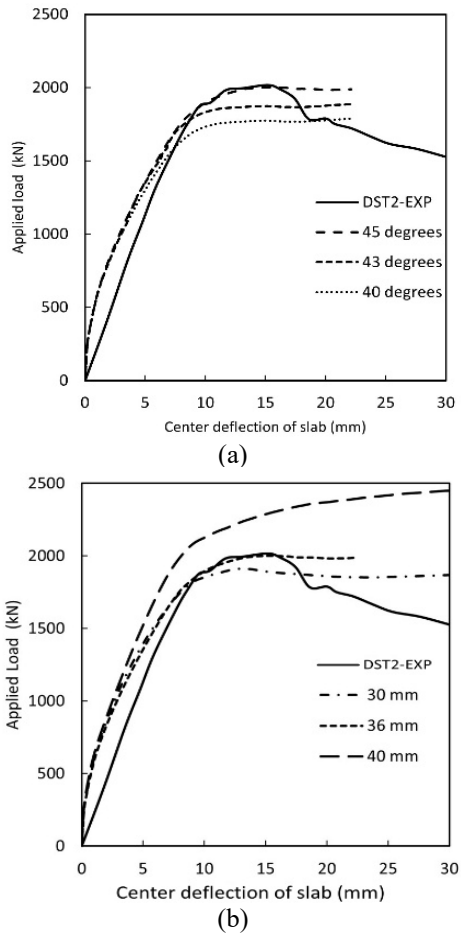

Figure 4. Sensitive analyses of slab model DST2 with (a) different deletion angles and mesh size 36 mm, and (b) with different mesh sizes and deletion angle 45°

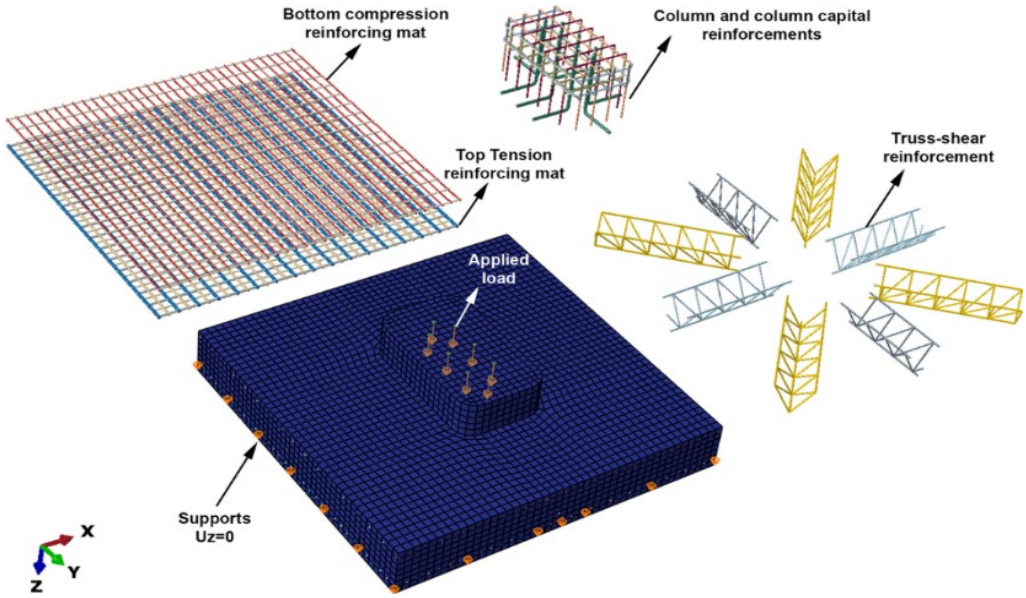

Figure 5. Typical geometry, boundary conditions, mesh configuration, and reinforcement details of slab models

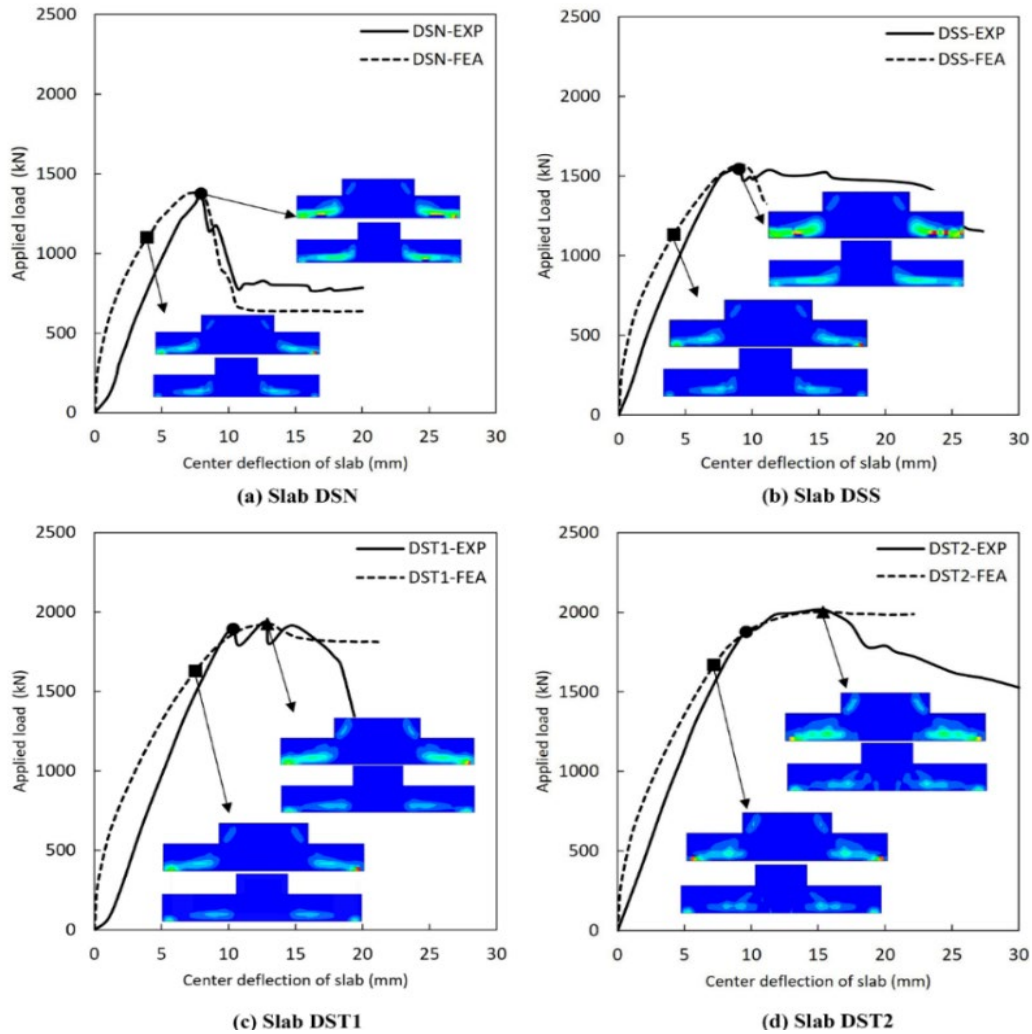

Figure 6. Load-deflection behaviour of slab models DSN, DSS, DST1, and DST2
Note: DSN: deep slab with no shear reinforcement, DSS: deep slab with single-leg stirrups, DST1, and DST2: deep slabs with trusses.

3.2 Discussion of calibration findings

Experimental results indicated a significant reduction in slab stiffness at the circular reference points, which correspond to punching shear crack locations. This reduction signifies a substantial widening of punching shear cracks at these points, suggesting that crack formation occurred much earlier in the loading process. Consequently, finite element analysis plays a

crucial role in visualising the early stages of punching shear crack development, as represented by the square reference points. For comparative purposes, the maximum load points are marked with triangles. Furthermore, the simulated slabs exhibited a stiffer response compared to their experimental counterparts due to the exclusion of temperature and shrinkage effects in the numerical model.

The strains in the flexural bars were measured exclusively for slab DSN during the experimental campaign. Both experimental and numerical observations confirmed that the flexural reinforcing bars did not yield at failure in slab DSN, indicating that the failure was due to pure punching shear. Eom et al. [26] speculated that flexural bars in slab DSS did not yield at failure, whereas yielding occurred at least in the x-direction for slabs DST1 and DST2. Finite element analysis indicated that specific flexural bars in slab DSS did experience yielding in the x-direction. In slabs DST1 and DST2, certain flexural bars demonstrated yielding in both the x- and y-directions upon failure. These findings highlight the significance of finite element analysis as a vital tool for revealing crucial details that may be neglected in experimental investigations.

The calibrated slab models exhibited punching shear failure beyond the column capital, despite the clear formation of crack patterns on the tension surface (see Figure 7). This is further supported by the presence of diagonal shear cracks, as shown in Figure 6. Also, the failure loads recorded for all slab models were lower than the ultimate flexural strength limit of 2382 kN assigned to them. Both slab models DST1 and DST2 demonstrated yielding in the first two diagonal bar trusses at failure; the other trusses showed insignificant stresses, indicating their minor role in resisting punching shear. Compared to experimental findings, only the first two rows of diagonal bars in slab DST1 yielded in the *y*-direction at failure. The single-leg stirrups in slab DSS experienced elevated stresses in the *y*-direction, though they remained below the specified yield stress.

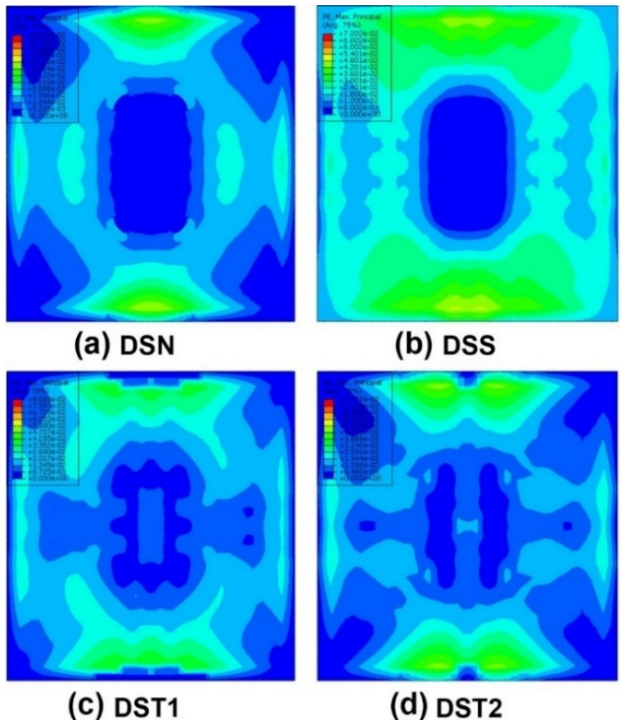

Figure 7. Cracking and failure modes on the tension surface of slab models
Note: DSN: deep slab with no shear reinforcement, DSS: deep slab with single-leg stirrups, DST1, and DST2: deep slabs with trusses.

The calibrated slab models exhibited conservative failure loads with a deviation of less than 5%. This is within the acceptable range for finite element analyses (≤ 20%), thereby confirming the reliability of these models for further investigations into shear-reinforced slabs utilising different types of truss-shear reinforcements. Table 3 displays the ultimate load and deflection at failure, as determined through finite element analysis and experimental testing.

Table 3. Comparison of failure loads between test and finite element analysis

Slab	Test Results		Finite Element Results	
	Failure Load (kN)	Displacement at Failure (mm)	Failure Load (kN)	Displacement at Failure (mm)
DSN	1361	8.00	1383	7.60
DSS	1543	9.00	1560	8.60
DST1	1939	12.7	1926	12.9
DST2	2029	15.0	2002	15.8

4. PARAMETRIC STUDIES

Parametric studies were performed to evaluate the role of trusses in improving the punching shear resistance of flat slabs. Slabs DST1 and DST2 were chosen as reference models for the study because they possess identical material properties and boundary conditions. For this analysis, six main types of trusses were considered (see Figure 8). Whilst various truss configurations can be used for punching shear reinforcement, these specific types were chosen because alternative designs tend to be overly congested with reinforcement bars, requiring a substantially thicker slab. The selected trusses range from triangular (T) to square (S) configurations. The trusses used in the parametric slab models maintained the same material properties as those in DST1 and DST2. Consequently, the parametric study was categorised into four groups based on specific evaluation criteria. Table 4 provides detailed information on all parametric slab models.

Group 1 comprises six slab models, each reinforced with two trusses (triangular or square) positioned orthogonally around the column capital, comparable to slab DST1. Group 2 consists of six slab models, each reinforced with eight trusses (triangular or square) arranged radially around the column capital, in accordance with the configuration of slab DST2. In both groups, the triangular and square trusses have an inclination angle θ_l of 49.3°, with a spacing of 130 mm between consecutive bars. Meanwhile, the angle θ_t is 59.2° for triangular trusses and 90° for square trusses. Table 4 lists the detailed specifications of all slab models in Groups 1 and 2.

Group 3 consists of four slab models. Two of these models

are shear-reinforced with two square trusses in each direction around the column capital, similar to slab DST1. The remaining two models are shear-reinforced with eight square trusses arranged radially around the column capital, resembling slab DST2. This group examines the effects of decreasing the spacing between adjacent bars. To accomplish this, the inclination angle θ_l is raised to 60° or 90° rather than 49.3°, while θ_t is adjusted to 90° instead of 59.2°. The spacing between successive bar trusses is therefore reduced to 90 mm, down from 130 mm. Truss types T2 and S2 are omitted from this category because of difficulties in practical implementation. Table 4 presents the specifications of all slab models within Group 3.

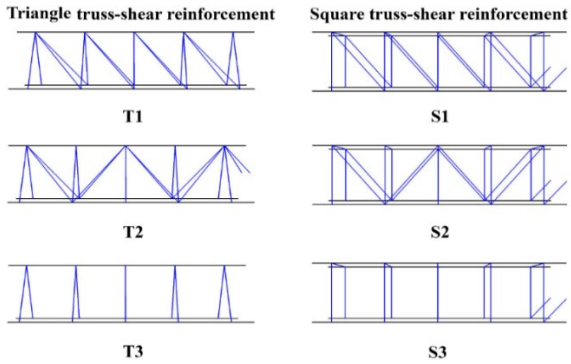

Figure 8. Truss-shear reinforcements adopted for parametric study

Table 4. Details of parametric slab models

Group No.	Slab Model	Arrangement Type	Truss Type	Spacing s (mm)	θ_l	θ_t	No. of Shear Bars within Critical Section
1	DST1-T1 (DST1-Finite Element Analysis (FEA))	Orthogonal	T1	130	49.3°	59.2°	16
	DST1-T2	Orthogonal	T2	130	49.3°	59.2°	16
	DST1-T3	Orthogonal	T3	130	49.3°	59.2°	16
	DST1-S1	Orthogonal	S1	130	49.3°	90°	16
	DST1-S2	Orthogonal	S2	130	49.3°	90°	16
	DST1-S3	Orthogonal	S3	130	49.3°	90°	16
2	DST2-T1 (DST2-FEA)	Radial	T1	130	49.3°	59.2°	16
	DST2-T2	Radial	T2	130	49.3°	59.2°	16
	DST2-T3	Radial	T3	130	49.3°	59.2°	16
	DST2-S1	Radial	S1	130	49.3°	90°	16
	DST2-S2	Radial	S2	130	49.3°	90°	16
	DST2-S3	Radial	S3	130	49.3°	90°	16
3	DST1-S1-60º	Orthogonal	S1	90	60°	90°	16
	DST1-S3-90º	Orthogonal	S3	90	90°	90°	16
	DST2-S1-60º	Radial	S1	90	60°	90°	16
	DST2-S3-90º	Radial	S3	90	90°	90°	16
4	I	Radial	S1	90	60°	90°	8
	II	Orthogonal	S1	90	60°	90°	8
	III	Orthogonal	S1	90	60°	90°	20
	IV	Radial	S1	90	60°	90°	8
	V	Orthogonal	S1	90	60°	90°	8
	VI	Orthogonal	S1	90	60°	90°	20
	VII	Radial	S1	90	60°	90°	16

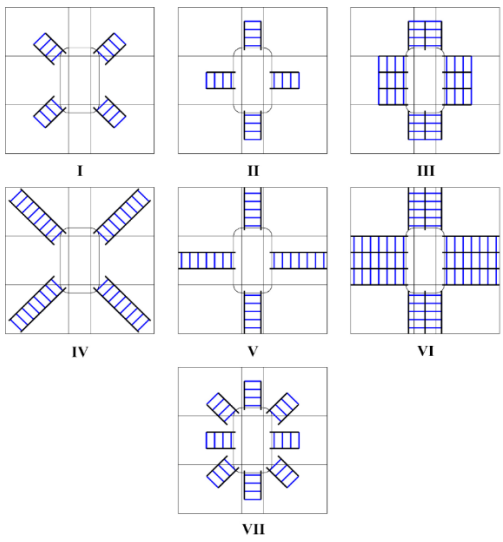

Figure 9. Different arrangements of square truss-shear reinforcement (type S1)

Group 4 evaluates the effectiveness of various square truss configurations with inclination angles of $\theta_l = 60°$ and $\theta_t = 90°$, as illustrated in Figure 9. Table 4 also provides detailed specifications of all slab models in Group 4.

5. RESULTS OF PARAMETRIC STUDIES

5.1 Punching strength and failure mode

In Group 1, the slab models DST1-T1, DST1-T2, and DST1-T3, which were shear-reinforced with two triangular trusses in each direction surrounding the column capital, exhibited similar behaviour and strength at failure (see Figure 10(a)). These models achieved an average increase of 29% in punching capacity compared to the control slab DSN. Conversely, the slab models DST1-S1, DST1-S2, and DST1-S3, which were shear-reinforced with two square trusses in each direction, also displayed similar responses and strength (see Figure 10(b)), resulting in an average enhancement of 46% in punching resistance compared to DSN. All slab models

in this group exhibited shear strengths below the ultimate flexural strength limit (V_{flex} = 2382 kN), indicating that they all failed due to punching shear beyond the column capital.

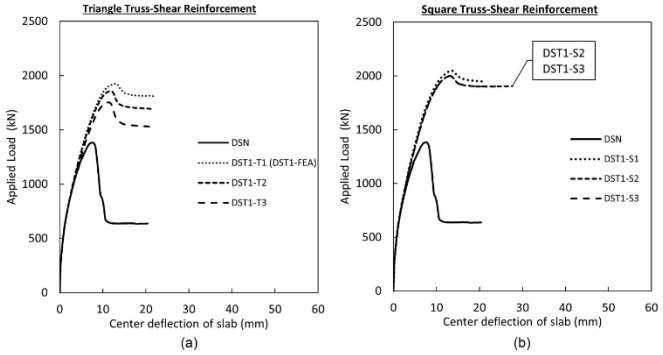

Figure 10. Load-deflection response of the slab models in Group 1

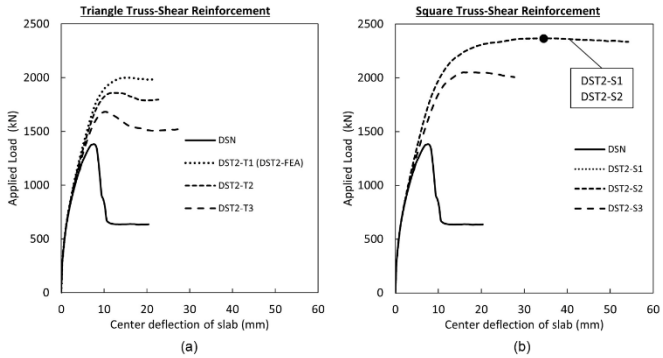

Figure 11. Load-deflection response of the slab models in Group 2

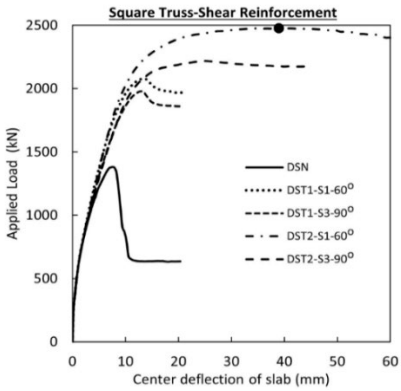

Figure 12. Load-deflection response of the slab models in Group 3

In Group 2, the slab models DST2-S1, DST2-S2, and DST2-S3, which were shear-reinforced with eight radially arranged square trusses around the column capital, exhibited better response and higher ultimate strength compared to DST2-T1, DST2-T2, and DST2-T3, which were shear-reinforced with triangular trusses (see Figure 11). Both DST2-S1 and DST2-S2 demonstrated similar behaviour and achieved an approximately 71% increase in punching strength compared to the control slab DSN. Furthermore, the shear strengths of all slab models in this group remained below the ultimate flexural strength limit (V_{flex} = 2382 kN), confirming that failure occurred due to punching shear beyond the column capital. Compared to Group 1, the radial arrangement of trusses proved to be more effective than the orthogonal arrangement in enhancing punching shear resistance.

In Group 3, the radial arrangement of square trusses (slab models DST2-S1-60° and DST2-S3-90°) demonstrated superior effectiveness compared to the orthogonal configuration (slab models DST1-S1-60° and DST1-S3-90°) in improving punching shear resistance (see Figure 12). The slab model DST2-S1-60° demonstrated superior performance, exceeding the ultimate flexural strength limit (V_{flex} = 2382 kN) with a failure load of 2478 kN, resulting in an approximate 79% increase in punching shear strength (see Figure 12). In comparison to Groups 1 and 2, the radial arrangement of truss type S1 with θ_l= 60° exhibited greater effectiveness than all other configurations with θ_l = 49.3°, regarding both punching shear strength and failure mode. However, square truss-shear reinforcements performed better than their triangular counterparts because they have four joints instead of three, and the presence of four chord bars increases stability and provides greater enhancement to the flexural bars.

In Group 4, slab models III, VI, and VII, which utilised trusses of type S1 with an inclination angle θ_l of 60°, exhibited increases in punching shear capacity of approximately 50%, 51%, and 53%, respectively. In contrast, other truss configurations proved to be less effective in enhancing punching shear strength (see Figure 13). All shear reinforcement configurations in this group ultimately resulted in punching shear failure across all slab models.

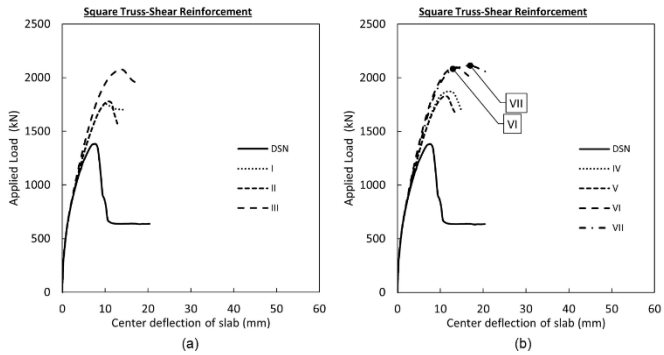

Figure 13. Load-deflection response of the slab models in Group 4

5.2 Crack patterns

All slab models exhibited distinct crack patterns on the tension surface upon failure. However, despite these variations, all models ultimately failed due to punching shear beyond the column capitals, except for the slab model DST2-S1-60°, which exhibited flexural failure. It is worth noting that the formation of well-defined crack patterns does not necessarily indicate flexural failure or the full mobilisation of flexural reinforcement. The majority of cracks were concentrated around the column capitals, just like the reference slabs (refer to Figure 7). The failure loads for each slab model are provided in Table 5.

5.3 Response of flexural and shear reinforcements

At failure, the number of yielded flexural reinforcement bars in the *x*-direction was greater than in the *y*-direction for all slab models. This is due to the lower flexural reinforcement ratio (ρ_{lx} = 0.009) and the unequal load transmission caused by the applied load being transferred through the rectangular

column capital. These findings confirm that shear forces and bending moments are higher along the shorter sides of the column capital compared to the longer sides. Table 5 presents the percentage of yielded flexural tension bars in both directions at failure. The data indicate that slab models featuring radial truss configurations exhibited a greater quantity of yielded flexural bars than those with orthogonal truss configurations. This occurs because a greater number of flexural bars engage with the chord bars in radial truss configurations, in contrast to slabs featuring solely orthogonal arrangements. This heightened interaction optimises the distribution of shear forces and bending moments throughout the slab, thereby enhancing overall structural performance. Consequently, these findings further illustrate the efficacy of the radial configuration of truss-shear reinforcements.

In slab models reinforced with truss types T1, T2, S1, and S2, all diagonal bar trusses oriented along the diagonal tension direction in the first two rows experienced yielding at failure across all models. Conversely, the other bar trusses had insignificant stresses, indicating their limited role in resisting punching shear. In slab models reinforced with truss types T3 and S3, the vertical bar trusses in the first two rows exhibited the greatest stress levels at failure. Moreover, the chord bars of the truss reinforcements in all slab models experienced negligible stresses at failure.

The truss-shear reinforcement was modelled based on the assumption that the concrete had a perfect bond with the shear reinforcement, which does not explicitly account for weld-joint behaviour. This assumption is plausible because of full welding and excellent anchorage. However, it is acknowledged that neglecting weld joint behaviour may affect local force redistribution. The negligible stresses noticed in some truss bars may be partly developed due to adopting such an assumption. However, the detailed modelling of truss joints is beyond the scope of the present study.

The numerical studies confirm the experimental findings, suggesting that weld joint failure may have occurred between the chord and diagonal bars of the triangular truss at failure. Furthermore, even under significant slab deflections, the vertical truss bars exhibited zero stress, indicating that they did not contribute to enhancing punching shear resistance. However, numerical analyses revealed that square trusses outperformed triangular trusses. This improvement is attributed to the increase in the angle θ_t (see Figure 1) from 59.2° in triangular trusses to 90° in square trusses. Consequently, this results in the formation of four weld joints instead of three, allowing for greater tensile stress resistance.

5.4 Stiffness, ductility, and energy absorption

The slopes of the load-deflection curves for all shear-reinforced slab models suggest that truss-shear reinforcements provided only a slight improvement in initial stiffness compared to the unreinforced slab model (DSN). This modest increase in stiffness is attributed to the minimal confinement pressure generated by the installation of truss reinforcements around the drop panel.

Table 5. Finite element results of parametric slab models

Group No.	Slab Model	Yielded Flexural Tension Bars (%)			Failure Load $V_{u,FEA}$ (kN)	Displacement at Failure (mm)	Load Increment (%)	Failure Mode	Energy Absorption (kN/mm)	Ductility Index δ_{max}/δ_y
		x-dir	*y*-dir	Total						
Ref. slabs	DSN-FEA	0	0	0	1382	8	0	Punching shear	7619	1.9
	DSS-FEA	3	0	1	1569	9	14	Punching shear	10420	2.11
	DST1-FEA	14	5	9	1753	11	27	Punching shear	15406	2.15
	DST2-FEA	32	8	20	2002	15	45	Punching shear	23345	2.54
1	DST1-T1 (DST1-FEA)	14	5	9	1926	11	27	Punching shear	17839	2.18
	DST1-T2	14	5	9	1855	12	34	Punching shear	15905	2.14
	DST1-T3	11	0	5	1753	11	27	Punching shear	15406	2.07
	DST1-S1	16	14	15	2047	13	48	Punching shear	19776	2.09
	DST1-S2	11	5	8	1999	13	45	Punching shear	18421	2.07
	DST1-S3	11	5	8	1999	13	45	Punching shear	18421	2.07
2	DST2-T1 (DST2-FEA)	32	8	20	2002	15	45	Punching shear	23345	2.54
	DST2-T2	22	5	14	1859	12	34	Punching shear	16271	2.18
	DST2-T3	16	5	11	1683	10	22	Punching shear	15602	2.2
	DST2-S1	70	41	55	2366	35	71	Punching shear	70828	4.47
	DST2-S2	65	38	51	2366	35	71	Punching shear	70828	4.47
	DST2-S3	49	11	30	2051	17	48	Punching shear	26020	2.43
3	DST1-S1-60°	16	27	22	2079	13	50	Punching shear	20023	2.09
	DST1-S3-90°	22	5	14	1979	13	43	Punching shear	18075	2.13
	DST2-S1-60°	73	70	72	2478	39	79	Flexural	82202	4.78
	DST2-S3-90°	65	19	42	2218	25	60	Punching shear	44401	3.29
4	I	27	0	14	1754	10	27	Punching shear	12769	1.92
	II	22	0	11	1778	11	29	Punching shear	13446	2.11
	III	27	19	23	2076	13	50	Punching shear	19738	2.06
	IV	32	0	16	1875	12	36	Punching shear	16113	1.74
	V	19	5	12	1828	11	32	Punching shear	18243	2.01
	VI	57	19	38	2098	14	52	Punching shear	26471	2.25
	VII	73	27	50	2113	17	53	Punching shear	26471	2.57

Additionally, all truss-shear reinforcement types significantly enhanced the ductility of the slabs compared to the unreinforced slab model (DSN). The slab models DST2-T1, DST2-S1, DST2-S2, DST2-S1-60°, DST2-S3-60°, and VII exhibited notable increases in ductility of approximately 34%, 135%, 135%, 152%, 73% and 35%, respectively, relative to DSN. The ductility of the slab models was evaluated using the ratio of deflection at ultimate load to deflection at yield load (δ_{max} / δ_y) [38, 39]. The ductility index is expressed as a dimensionless ratio, where the yield load is assumed to be 75% of the ultimate load [40]. The ductility indexes for all slab models are presented in Table 5.

Furthermore, all truss-shear reinforcement types significantly improved the energy absorption capacity of the slabs compared to the unreinforced slab model (DSN), as indicated by the area under the load-deflection curves. The slab models DST2-T1, DST2-S1, DST2-S2, DST2-S1-60°, DST2-S3-60°, and VII exhibited significant increases in energy absorption of nearly 206%, 135%, 830%, 830%, 979%, 483% and 247%, respectively, relative to DSN. The energy absorption indexes for all slab models are summarised in Table 5.

6. CODES EVALUATION

The nominal punching shear strengths V_n specified in the ACI 318-19 and Eurocode 2 design codes were compared with the ultimate failure loads $V_{u,\ FEA}$ of the slab models. The nominal punching shear strength for slabs with shear reinforcement is defined in each design code as follows:

According to ACI 318-19,

$$V_{n,ACI} = 0.5V_{c,ACI} + V_s \tag{2}$$

where,

$$V_{c,ACI} = min\left\{\left(\frac{1}{3}\right), \left(0.17 + \frac{0.33}{\beta}\right), \left(0.17 + \frac{0.083\alpha_s d}{b_o}\right)\right\} \lambda_s \lambda \sqrt{f_c'} b_o d$$

$$\lambda_s = \sqrt{2/(1 + 0.004d)} \leq 1$$

$$V_s = \left(A_v f_{yt} d/s\right)(cos\ \theta_l + sin\ \theta_l)(sin\ \theta_t)$$

$$b_o = 2(c_x + c_y - 4r) + \pi(2r + d)$$

According to Eurocode 2,

$$V_{n,EC2} = 0.75V_{c,EC2} + V_{se} \tag{3}$$

where,

$$V_{c,EC2} = 0.18k(100\rho f_{ck})^{1/3} b_o d \geq V3/2\sqrt{f_{ck}}_{o\,min}$$

$$k = 1 + \sqrt{200/d} \leq 2$$

$$V_{se} = \left(1.5A_v f_{yte} d/s\right)(cos\ \theta_l + sin\ \theta_l)(sin\ \theta_t)$$

$$f_{yte} = 1.15(250{+}0.25\mathrm{d}) \leq f_{yt}$$

$$b_o = 2(c_x + c_y - 4r) + \pi(2r + 4d)$$

In Eqs. (2) and (3), d denotes the effective slab depth, whilst λ_s represents the size effect factor. The parameter λ is taken equal to 1 for normal-weight concrete. The variable r refers to the column capital corner radius, and A_v represents the area of shear reinforcement located along the critical perimeter b_o. In addition, s indicates the spacing between consecutive bar trusses, whereas ρ refers to the average tension reinforcement ratio of the slab in both the x- and y-directions. Finally, c_y and c_x correspond to the longer and shorter dimensions of the rectangular column capital, respectively.

In ACI 318-19, the concrete contribution to punching shear strength is limited to 50% ($0.5V_{c,ACI}$), as expressed in Eq. (2), whilst the shear reinforcement contribution corresponds to the yield force. This implies that the punching shear strength in ACI 318-19 is determined based on its maximum load capacity after the shear reinforcement has yielded. In contrast, Eurocode 2 (Eq. (3)) limits the concrete contribution to 75% ($0.75V_{c,EC2}$) and defines the shear reinforcement contribution as a function of the effective yield stress (f_{yte}). This suggests that Eurocode 2 evaluates punching shear strength before the shear reinforcement yields. Furthermore, the critical perimeter is defined at $0.5d$ from the column capital face in ACI 318-19, whereas in Eurocode 2, it is positioned at $2d$ from the column capital face.

Table 6 presents the nominal punching shear strengths V_n estimated using Eqs. (2) and (3). The material and geometric parameters used in the punching shear strength calculations are as follows: f'_c = 31.8 MPa for DSN and DSS, and 32.4 MPa for all parametric slab models, d = 206 mm, ρ = 0.0126, r = 90 mm, c_y = 720 mm, c_x = 420 mm, α_s = 40, and β = 720/420.

For the slab model DSN, the nominal shear strength V_n was defined as the shear strength contributed solely by the concrete, expressed as $V_n = V_c$. The estimation of V_s or V_{se} in all shear-reinforced slab models (including those reinforced with trusses and stirrups) was conducted by applying the yield strength limits prescribed in the design codes. For slab models reinforced with trusses of types T1, T2, S1, and S2, only the diagonal bars (D8), which experienced significant stresses at failure, were considered in the computation of V_s and V_{se}, whilst the vertical bars were excluded due to their negligible recorded stresses at failure. Since the diagonal bars were inclined at an angle θ_l relative to the longitudinal direction, V_s and V_{se} were amplified by a factor of (sin θ_l + cos θ_l) (refer to Figure 1). In addition, considering the inclination angle θ_t relative to the transverse direction, V_s and V_{se} were reduced by a factor of sin θ_t. Conversely, for slab models reinforced with trusses of types T3 and S3, V_s and V_{se} were only reduced by multiplying by sin θ_t. To ensure compliance with design standards, the calculations of V_s and V_{se} were based on the design yield stress limits (420 MPa for ACI 318-14 and 347 MPa for Eurocode 2) rather than the actual yield strengths of the reinforcement.

Table 6 shows a comparison between the punching shear strengths that are predicted by design codes ($V_{n,ACI}$ and $V_{n,EC2}$) and the punching shear strengths that are numerically estimated ($V_{u,FEA}$). When it came to predicting punching shear strengths, it seemed that ACI 318-19 was more conservative than Eurocode 2.

In the predictions for ACI 318 and EC2, only the diagonal truss bars were incorporated, as the vertical bars demonstrated minimal stress at failure. This signifies that the vertical bars did not enhance the punching shear strength, and their contribution is limited to adding additional stability to the truss system. This selective inclusion is recognised as a

simplification, as the formulations of the design codes presume that all shear reinforcement contributes. Consequently, the code predictions provided here should be regarded as somewhat conservative and indicative.

Table 6. Punching strengths predicted by ACI 318-19 and Eurocode 2

Group	Slab Model	ACI 318-19 (kN)			Eurocode 2 (kN)			Comparison with Test Results		
		$V_{c,ACI}$	V_s	$V_{n,ACI}$	$V_{c,EC2}$	V_{se}	$V_{n,EC2}$	$V_{u,FEA}$ (kN)	$V_{u,FEA} / V_{n,ACI}$	$V_{u,FEA} / V_{n,EC2}$
Ref. slabs	DSN-FEA	1073	0	1073	1183	0	1183	1382	1.29	1.17
	DSS-FEA	1073	864	1400	1183	1070	1957	1569	1.12	0.80
	DST1-FEA	1083	647	1189	1190	802	1695	1926	1.62	1.14
	DST2-FEA	1083	647	1189	1190	802	1695	2002	1.68	1.18
1	DST1-T1 (DST1-FEA)	1083	647	1189	1190	802	1695	1926	1.62	1.14
	DST1-T2	1083	647	1189	1190	802	1695	1855	1.56	1.09
	DST1-T3	1083	460	1001	1190	570	1462	1753	1.75	1.20
	DST1-S1	1083	754	1295	1190	934	1827	2047	1.58	1.12
	DST1-S2	1083	754	1295	1190	934	1827	1999	1.54	1.09
	DST1-S3	1083	535	1076	1190	662	1555	1999	1.86	1.29
2	DST2-T1 (DST2-FEA)	1083	647	1189	1190	802	1695	2002	1.68	1.18
	DST2-T2	1083	647	1189	1190	802	1695	1859	1.56	1.10
	DST2-T3	1083	460	1001	1190	570	1462	1683	1.68	1.15
	DST2-S1	1083	754	1295	1190	934	1827	2366	1.83	1.30
	DST2-S2	1083	754	1295	1190	934	1827	2366	1.83	1.30
	DST2-S3	1083	535	1076	1190	662	1555	2051	1.91	1.32
3	DST1-S1-60°	1083	1089	1630	1190	1349	2242	2079	1.28	0.93
	DST1-S3-90°	1083	772	1314	1190	957	1849	1979	1.51	1.07
	DST2-S1-60°	1083	1089	1630	1190	1349	2242	2478	1.52	1.11
	DST2-S3-90°	1083	772	1314	1190	957	1849	2218	1.69	1.20
4	I	1083	544	1086	1190	675	1567	1754	1.62	1.12
	II	1083	544	1086	1190	675	1567	1778	1.64	1.13
	III	1083	1361	1902	1190	1687	2579	2076	1.09	0.80
	IV	1083	544	1086	1190	675	1567	1875	1.73	1.20
	V	1083	544	1086	1190	675	1567	1828	1.68	1.17
	VI	1083	1361	1902	1190	1687	2579	2098	1.10	0.81
	VII	1083	1089	1630	1190	1349	2242	2113	1.30	0.94
		Average							1.57	1.12
		Standard Deviation							0.229	0.142
		Coefficient of variation (%)							14.61	12.71

7. CONCLUSIONS

Non-linear finite element analyses were performed using the ABAQUS software package to investigate the punching shear response of slabs supported by rectangular columns with attached capitals, which experienced asymmetric shear transmission in both orthogonal directions. Different types of truss-shear reinforcements were strategically placed around the column capitals to improve the punching shear resistance of the flat slabs.

The concrete damage plasticity model in ABAQUS accurately predicted the true strength and behaviour of the tested shear-reinforced slabs, with deviations of less than 5%. The incorporation of truss-shear reinforcements significantly enhanced the punching strength, stiffness, ductility, and energy absorption of the flat slabs. In truss types T1, T2, S1, and S2, the first two diagonal bars oriented in the direction of diagonal tension reached their yield stress at failure, whilst the vertical and diagonal bars exhibited negligible stress. Conversely, in truss types T3 and S3, the vertical bars recorded stress levels at failure that were below the designated yield strength.

In all shear-reinforced slab models at failure, more flexural bars yielded in the *x*-direction than in the *y*-direction. This was due to the uneven load transfer in both directions and the lower flexural reinforcement ratio in the *x*-direction. Moreover, slabs reinforced with radially arranged trusses exhibited a higher number of yielded flexural bars compared to those with orthogonally arranged trusses. Therefore, it is highly recommended to adopt a radial arrangement of trusses around rectangular columns and capitals to enhance structural performance.

Truss-shear reinforcement proved effective in altering the failure mode of flat slabs from punching shear to flexural failure. The likelihood of flexural failure increases with a larger angle θ_l and adopting square trusses (type S1). At failure, all slab models exhibited distinct crack patterns on the tension surface around the column capitals, with most failing in punching shear mode. However, the slab model DST-S1-60° was an exception, demonstrating a flexural failure mode.

The design methods outlined in ACI 318-19 and Eurocode 2 provided conservative estimates of the punching shear strengths for shear-reinforced flat slabs with truss bars supported by rectangular column capitals. Whilst Eurocode 2 overestimated the punching strength for certain slabs, ACI 318-19 proved to be more conservative overall. These code-based estimations were derived by excluding the contribution of non-essential bar trusses and applying the allowable design yield stress for shear reinforcement.

ACKNOWLEDGMENT

The authors acknowledge the funding support of Research University Grant (Grant No.: GUP-2022-021), Universiti Kebangsaan Malaysia, and facilities provided by both institutions.

REFERENCES

[1] Milligan, G.J., Polak, M.A., Zurell, C. (2020). Finite element analysis of punching shear behaviour of concrete slabs supported on rectangular columns. Engineering Structures, 224: 111189. https://doi.org/10.1016/j.engstruct.2020.111189

[2] Šarvaicová, S., Borzovič, V., Halvonik, J. (2024). Experimental investigation of punching shear behavior of flat slabs supported by rectangular columns and loaded with various load patterns. Structural Concrete, 25(2): 1404-1417. https://doi.org/10.1002/suco.202201251

[3] Sagaseta, J., Tassinari, L., Fernández Ruiz, M., Muttoni, A. (2014). Punching of flat slabs supported on rectangular columns. Engineering Structures, 77: 17-33. https://doi.org/10.1016/j.engstruct.2014.07.007

[4] Teng, S., Chanthabouala, K., Lim, D.T.Y., Hidayat, R. (2018). Punching shear strength of slabs and influence of low reinforcement ratio. ACI Structural Journal, 115(1): 139-150. https://doi.org/10.14359/51701089

[5] ACI Committee. (2019). ACI 318-19: Building code requirements for structural concrete. Farmington Hills, MI: American Concrete Institute. https://mattia.ir/wp-content/uploads/2020/10/ACI-318R-19.pdf.

[6] Fernández Ruiz, M., Mirzaei, Y., Muttoni, A. (2013). Post-punching behavior of flat slabs. Structural Concrete, 110: 801-812.

[7] Cavagnis, F., Fernández Ruiz, M., Muttoni, A. (2018). An analysis of the shear-transfer actions in reinforced concrete members without transverse reinforcement based on refined experimental measurements. Structural Concrete, 19(1): 49-64. https://doi.org/10.1002/suco.201700145

[8] Ghali, A., Gayed, R.B. (2018). Punching shear strength of slabs and influence of low reinforcement ratio. ACI Structural Journal, 115(6): 1815-1816. https://www.proquest.com/openview/990d8584fd3ece0cdd098c360912fe9e/1?pq-origsite=gscholar&cbl=36963.

[9] Regan, P.E. (1974). Design for punching shear. The Institution of Structural Engineers, 52(6): 197-207. https://www.istructe.org/journal/volumes/volume-52-(published-in-1974)/issue-6/design-for-punching-shear/.

[10] Regan, P.E., Braestrup, M.W. (1985). Punching Shear in Reinforced Concrete: A State of Art Report. Issue 168 of Bulletin d'information / Comité euro-international du béton, Euro-International Committee for Concrete, Secretariat Permanent. https://books.google.com.sg/books?id=IPn2cQAACAAJ.

[11] CEN. (2004). Eurocode 2: Design of concrete structures - Part 1-1: General rules and rules for buildings (EN 1992-1-1:2004). Brussels: European Committee for Standardization.

[12] Nayef, S., Zaki, W., Rabie, M. (2019). Effect of reinforcement on punching shear behavior of flat slabs. International Journal of Civil Engineering and Technology, 10(2): 2403-2418. https://iaeme.com/Home/article_id/IJCIET_10_02_238.

[13] Broms, C.E. (2007). Ductility of flat plates: Comparison of shear reinforcement systems. ACI Structural Journal, 104(6): 703-711. https://doi.org/10.14359/18952

[14] Caldentey, A.P., Lavaselli, P.P., Peiretti, H.C., Fernandez, F.A. (2013). Influence of stirrup detailing on punching shear strength of flat slabs. Engineering Structures, 49: 855-865. https://doi.org/10.1016/j.engstruct.2012.12.032

[15] Broms, C.E. (2019). Cages of inclined stirrups as shear reinforcement for ductility of flat slabs. ACI Structural Journal, 116(1): 83. https://doi.org/10.14359/51710871

[16] Almeida, A.F.O., Alcobia, B., Ornelas, M., Marreiros, R., Ramos, A.P. (2020). Behaviour of reinforced-concrete flat slabs with stirrups under reversed horizontal cyclic loading. Magazine of Concrete Research, 72(7): 339-356. https://doi.org/10.1680/jmacr.18.00209

[17] Raafat, A., Fawzi, A., Metawei, H., Abdalla, H. (2021). Assessment of stirrups in resisting punching shear in reinforced concrete flat slab. HBRC Journal, 17(1): 61-76. https://doi.org/10.1080/16874048.2021.1881422

[18] Bompa, D.V., Elghazouli, A.Y. (2017). Numerical modelling and parametric assessment of hybrid flat slabs with steel shear heads. Engineering Structures, 142: 67-83. https://doi.org/10.1016/j.engstruct.2017.03.070

[19] Bompa, D.V., Elghazouli, A.Y. (2016). Structural performance of RC flat slabs connected to steel columns with shear heads. Engineering Structures, 117: 161-183. https://doi.org/10.1016/j.engstruct.2016.03.022

[20] Bompa, D.V., Elghazouli, A.Y. (2020). Nonlinear numerical simulation of punching shear behavior of reinforced concrete flat slabs with shear-heads. Frontiers of Structural and Civil Engineering, 14: 331-356. https://doi.org/10.1007/s11709-019-0596-5

[21] Tan, Y., Teng, S. (2005). Interior slab-rectangular column connections under biaxial lateral loadings. ACI Special Publication, 232: 147-174. https://doi.org/10.14359/14941

[22] Dam, T.X., Wight, J.K. (2016). Flexurally-triggered punching shear failure of reinforced concrete slab–column connections reinforced with headed shear studs arranged in orthogonal and radial layouts. Engineering Structures, 110: 258-268. https://doi.org/10.1016/j.engstruct.2015.11.050

[23] Park, H.G., Kim, Y.N., Song, J.K., Kang, S.M. (2001). Lattice shear reinforcement for enhancement of slab–column connections. Journal of Structural Engineering, 138(3): 425-437. https://doi.org/10.1061/(ASCE)ST.1943-541X.0000484

[24] Park, H.G., Ann, K.S., Choi, K.K., Chung, L. (2007). Lattice shear reinforcement for slab–column connections. ACI Structural Journal, 104(3): 294-303.

[25] Kang, S.M., Park, H.G., Kim, Y.N. (2013). Lattice-reinforced slab–column connections under cyclic lateral loading. ACI Structural Journal, 110(6): 929-939. https://doi.org/10.14359/51686149

[26] Eom, T.S., Song, J.W., Song, J.K., Kang, G.S., Yoon, J.K., Kang, S.M. (2017). Punching-shear behavior of slabs with bar truss shear reinforcement on rectangular columns. Engineering Structures, 134: 390-399. https://doi.org/10.1016/j.engstruct.2016.12.048

[27] Dassault Systems Simulia Corp. (2014). ABAQUS

analysis user's manual 6.14-EF. Providence, RI: Dassault Systems Simulia Corp.
[28] Rasoul, Z.M.R.A., Taher, H.M.A.M. (2019). Accuracy of concrete strength prediction behavior in simulating punching shear behavior of flat slab using finite element approach in Abaqus. Periodicals of Engineering and Natural Sciences, 7(4): 1933-1949. https://doi.org/10.21533/pen.v7i4.848
[29] Akinpelu, M.A., Gabriel, D.S., Salman, A.M., Raheem, I.A. (2023). Numerical study on the effect of different column shapes on punching shear behavior of flat slabs. Results in Engineering, 19: 101345. https://doi.org/10.1016/j.rineng.2023.101345
[30] Genikomsou, A.S., Polak, M.A. (2015). Finite element analysis of punching shear of concrete slabs using damaged plasticity model in ABAQUS. Engineering Structures, 98: 38-48. https://doi.org/10.1016/j.engstruct.2015.04.016
[31] Panahi, H., Genikomsou, A.S. (2022). Comparative evaluation of concrete constitutive models in non-linear finite element simulations of slabs with different flexural reinforcement ratios. Engineering Structures, 252: 113617. https://doi.org/10.1016/j.engstruct.2021.113617
[32] Taresh, H.R., Al Hussein, T.H.A., Radzi, A., Yatim, M.Y.M. (2025). Numerical modeling of perforated flat slabs strengthened with angle plates. Structural Concrete, 26(6): 7943-7956. https://doi.org/10.1002/suco.70150
[33] Taresh, H.R., Yatim, M.Y.M., Azmi, M.R. (2021). Finite element analysis of interior slab–column connections strengthened by steel angle plates. Structural Concrete, 22(2): 676-690. https://doi.org/10.1002/suco.201900561
[34] Taresh, H.R., Yatim, M.Y.M., Azmi, M.R. (2021). Punching shear behaviour of interior slab–column connections strengthened by steel angle plates. Engineering Structures, 238: 112246. https://doi.org/10.1016/j.engstruct.2021.112246
[35] Ali, Y.A., Assi, L.N., Abas, H., Taresh, H.R., Dang, C.N., Ghahari, S. (2023). Numerical investigation on effect of opening ratio on structural performance of reinforced concrete deep beam reinforced with CFRP enhancements. Infrastructures, 8(1): 2. https://doi.org/10.3390/infrastructures8010002
[36] Comité Euro-International du Béton. (1993). CEB-FIP Model Code 1990: Design Code. London: Thomas Telford.
[37] Amirkhani, S., Lezgy-Nazargah, M. (2021). Nonlinear finite element analysis of reinforced concrete columns: Evaluation of different modeling approaches for considering stirrup confinement effects. Structural Concrete, 23(5): 2820-2836. https://doi.org/10.1002/suco.202100532
[38] Wang, Z.B., Tao, Z., Han, L.H., Uy, B., Lam, D., Kang, W.H. (2017). Strength, stiffness and ductility of concrete-filled steel columns under axial compression. Engineering Structures, 135: 209-221. https://doi.org/10.1016/j.engstruct.2016.12.049
[39] Cavaco, E., Pacheco, I., Camara, J. (2018). Detailing of concrete-to-concrete interfaces for improved ductility. Engineering Structures, 156: 210-223. https://doi.org/10.1016/j.engstruct.2017.10.058
[40] Park, R. (1988). Ductility evaluation from laboratory and analytical testing. In Proceedings of the 9th World Conference on Earthquake Engineering, Tokyo, Japan, pp. 605-616. https://www.iitk.ac.in/nicee/wcee/article/9_vol8_605.pdf.